RSC Advances

PAPER

View Article Online
View Journal | View Issue

Cite this: *RSC Adv.*, 2021, **11**, 4407

Adsorption behavior of gardenia yellow pigment on embedded spherical cellulose adsorbent

Jianting Liu,[ab] Zhendong Yu,[a] Qiqi Li,[a] Yuancai Lv,[a] Chunxiang Lin,[a] Jianhui Huang,[b] Yifan Liu*[ab] and Minghua Liu*[a]

Received 18th November 2020
Accepted 26th December 2020

DOI: 10.1039/d0ra09796a

rsc.li/rsc-advances

A spherical cellulose adsorbent embedded with black wattle extract (SABW) was prepared by an inverse suspension method, and used to adsorb the typical food pigment, gardenia yellow pigment (GYP). Results of SEM, XRD, FTIR and BET characterization showed that SABW was composed of abundant porous structures and functional groups such as –C=O, –OH and benzene ring groups. The batch adsorption experiments revealed that SABW presented excellent adsorption performance for GYP with a high adsorption percentage of 97.96%. The adsorption process followed the Langmuir and Freundlich adsorption isotherm, and the experimental data were in good agreement with the pseudo-second order dynamic model. Furthermore, the main adsorption mechanism involved hydrogen bonding, electrostatic interaction and pore adsorption. Importantly, the desorption and regeneration experiments showed that SABW had satisfactory reusability and retained 92.30% adsorption after 4 cycles. The above results provide a vital theoretical basis for the extraction of GYP.

1 Introduction

Gardeniae Fructus is a traditional Chinese medicine which has been commonly used in the treatment of jaundice hepatitis, contusion, hypertension and diabetes.[1–4] It has demonstrated effective pharmacological activities such as removing activity, inhibiting apoptosis of cells, and protecting activity against oxidative damage.[5–8] Gardenia yellow pigment (GYP) is one of the main active substances of Gardeniae Fructus. It has medicinal effects similar to Gardeniae Fructus and is commonly used as a nutritive colorant.[9] GYP is widely used as a food pigment in beverages, pastries, instant noodles and cooked food due to its water solubility.[10,11] Therefore, the extraction technologies of GYP from Gardeniae Fructus play an important role in improving the quality of GYP and promoting the development of gardenia. So far, the main extraction methods of GYP from gardenia include general extraction,[10] microwave extraction,[12] supercritical extraction[13] and so on. However, the products contain a large amount of impurities after the general extraction process, and cannot be used directly. Hence, it is necessary to refine the crude GYP. The main refining methods of GYP include macroporous resin adsorption methods, membrane extraction and separation methods, enzyme refining methods, gel chromatography methods and so on.[14–16] Some methods are not suitable for mass production due to the number of organic solvents and heavy work, and some have the shortcomings of large amounts of organic residues and poor separation effects. As a result, it is of great significance to develop an efficient adsorption material for GYP refining.

Tannins as a natural biomass, have a series of unique chemical properties, such as reducibility, the active of capturing free radical, the amphiphilic structure,[17] which can be used as an alternative and efficient adsorbent for the multiple adjacent hydroxyl groups.[18,19] However, tannins often exist in an amorphous state and are easily soluble in water, ethanol, propanol and other solvents. Thus, they cannot be used as water treatment materials directly and must be modified or immobilized in the medium.[20]Many researchers have studied the modified and immobilized of tannin, the adsorbents were applied to the adsorption of protein, amino acid, ethanol, iron ion, chromium ion and so on.[21,22] According to the previous investigations, cellulose is the most suitable carrier for the immobilization of tannins,[23–25] because cellulose adsorbent not only has the adsorption capacity of microbial adsorption, but also displays higher stability and better selectivity than resin adsorption method. At the same time, cellulose adsorbent has many advantages, such as wide sources, low cost, biodegradability and environmentally friendly. Formerly, a variety of cellulose-based adsorbents have been prepared to remove different pollutants. For example, Jilal *et al.* was grafting of EDTA on hydroxyethyl cellulose to remove Pb(II) and Cu(II) from aqueous solutions.[26] Tian *et al.* modified cellulose with graphene oxide to remove rhodamine B from aqueous solutions.[27] In addition, Zhang investigated the adsorption properties of polymyxin B

[a]*Fujian Provincial Engineering Research Center of Rural Waste Recycling Technology, College of Environment and Resources, Fuzhou University, Fuzhou 350116, Fujian, China. E-mail: yfanym@163.com; mhliu2000@fzu.edu.cn*

[b]*Fujian Provincial Key Laboratory of Ecology-Toxicological Effects and Control for Emerging Contaminants, College of Environmental and Biological Engineering, Putian University, Putian, 351100, Fujian, China*

immobilized on cross-linked cellulose in aqueous solutions containing the toxic endotoxin.[28] Therefore, it is significant to make full use of the earth's most abundant renewable resources in the preparation of cellulose absorbents, especially as a carrier of tannin for the good adsorption properties.

In this work, the performance of GYP extract from aqueous solution on spherical cellulose adsorbent embedded with black wattle extract (SABW) was studied. The adsorption conditions were optimized and adsorption kinetics and thermodynamic were investigated to understand the general adsorption's regulation of SABW. To better understand the adsorption mechanism of GYP, the particles were characterized with SEM, XRD, FTIR and its surface area. In addition, the desorption and regeneration conditions of GYP were optimized to obtain relevant parameters. These provided relevant basis for the application and research of adsorbents in the field of food. The novelty of the paper was that the preparation process of SABW was simple, and the adsorption process for GYP had high separation efficiency and low residual concentration.

2 Experimental section

2.1 Materials

Masson pine kraft pulp cellulose (MPC) was obtained from Nanping Paper Industry Co., Ltd, Fujian, China. Gardenia yellow pigment was purchased from Chengdu University of Traditional Chinese Medicine. Black wattle extract was provided by Guangxi Wuming Black Wattle Extract Factory Co., Ltd. $CaCO_3$ was purchased from Sinopharm Chemical Co., Ltd. All other agents in this work were of analytical grade and used without further purification. Deionized water was used throughout the work.

2.2 Synthesis of the adsorbent

2.2.1 Preparation of viscose. 20.0 g of MPC was soaked in 20% NaOH solution at room temperature for 2 h. The excess alkali liquor was extruded until the remaining alkali cellulose was about 100 g, and the optimum viscosity was obtained by aging at room temperature for 3.0 days. The alkali cellulose was put into a 500 mL three-necked flask with 9.1 mL of CS_2. After stirring the mixture for a while, 210 mL of 6 wt% NaOH solution and 0.028 g of sodium oleate (as surfactant) were added. The mixture was stirred for 3 h at room temperature to obtain viscose, then it was removed, sealed and placed under dark conditions for 1 day for standby application.

2.2.2 Preparation of SABW. The polymer phase was obtained by adding 30 mL of viscose, 2.0 g of $CaCO_3$ and 0.3 g of imbedding agent black wattle extract (it contains tannins) into a 500 mL three-necked flask. After 10 minutes of polymer phase stirring, 120 mL of dispersed phase transformer oil was added, as well as 30 mL of distilled water and a small amount of dispersant sodium oleate. After dispersing evenly in 200 rpm stirring, the mixture was slowly heated to 65 °C and reacted for 1.5 h. After the reaction, the water bath was removed and the system was naturally cooled to room temperature under agitation. The oil phase of the upper layer was recovered, and the lower oil phase containing brown beads is filtered. The brown beads being wished which were identified as embedded spherical cellulose adsorbent with black wattle extract (SABW). In addition, the spherical cellulose adsorbent without black wattle extract (SCB) was prepared for the experimental comparison.

2.3 Characterizations

The scanning electron microscope (SEM, SUPRA 55; Carl Zeiss Jena, Germany) was used to analyze the morphologies and sizes of MPC and SABW. The change of crystal structure of MPC before and after modification was characterized by X-ray diffraction (XRD, D8 advance; Bruker, Karlsruhe, Germany). The Fourier transform infrared (FTIR) spectra of MPC and SABW were received using a Nicolet AVATAR 360 FTIR spectrometer (Thermo Nicolet Corp., Waltham, USA). The specific surface area, pore size and pore volume were obtained by Brunauer–Emmett–Teller equation (BET, ASAP 2020 HD88; Micromeritics, Georgia, USA).

2.4 Adsorption studies

The static adsorption experiments were conducted by shaking 0.2 g of SABW with different concentrations (160–260 mg L^{-1}) of GYP and pH values (1–10, adjusted with 1 mol L^{-1} NaOH or HCl solutions) in conical flask for 20–180 min. After equilibrium, the concentrations of GYP in the flask were determined by High Efficiency Liquid Chromatography (HPLC, HITACHI L-2000) means with Ultimate 5 μm XB-C18 (4.6 × 250 mm) and mobile phase employ by acetonitrile–ultrapure water (80 : 20) at a flow velocity of 0.8 mL min^{-1}.[29] The adsorption capacity of GYP adsorbed by SABW, q_e (mg g^{-1}), was obtained as follows (eqn (1)),

$$q_e = (C_0 - C_e) \times V/W \quad (1)$$

where C_0 and C_e (mg L^{-1}) are the initial and equilibrium concentrations of GYP, respectively, V is the volume of solution (L), and W is the weight of SABW (g).

The used adsorbent after adsorption was washed twice with 80% methanol and ethanol followed by distilled water several times to remove adsorbed GYP. It was reused for further adsorption. All adsorption experiments were repeated three times to ensure the accuracy of the data, and the results were expressed in terms of average values.

3 Results and discussion

3.1 Characterization of MPC and SABW

The morphological characteristics of MPC and SABW were observed by SEM (Fig. 1). Compared with MPC (Fig. 1(a–c)), SABW displayed 3-D spherical structure with well-developed pore structure, indicating the substantial morphology change of MPC after the hydroxyl groups interact.[30] In addition, the MPC had a smooth surface, while SABW had flat and rough surface, which was conducive to the adsorption of GYP.

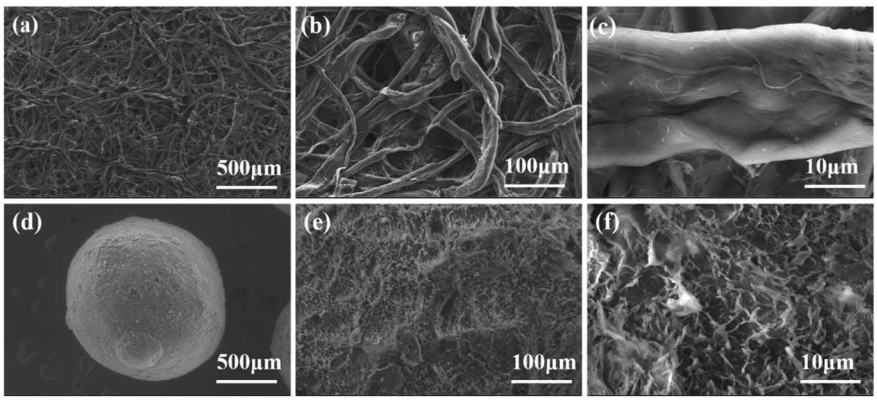

Fig. 1 SEM images of MPC (a–c), SABW (d–f).

Cellulose molecules can be divided into crystalline and non-crystalline regions in structure. The change of crystal structure of the MPC and SABW was analyzed by X-ray diffraction (Fig. 2(a)). It showed that MPC presented type I structure, which 2θ was 14.48°, 16.06°, 22.38° and 34.02° respectively corresponding to type I on the crystal structure of (101), (10$\bar{1}$), (002) and (040) face.[31] Meanwhile, XRD spectra of SABW presented a type II structure, whose 2θ was approximately 20° and 22° respectively corresponding to type II on the crystal structure of (101) and (10$\bar{1}$),[32] indicating that the crystal structure of MPC was changed obviously. As a result, the type I structure of MPC was successfully changed to type II structure. In addition, the diffraction peak at 22.38° of MPC had strongest peak, while the diffraction peak strength of SABW decreased, implying that the crystal structure of MPC was regular, and the crystal structure of SABW was destroyed.[33] The higher the destruction of the crystal structure, the more complete the reaction of synthetic cellulose.[33] At the same time, the diffraction peak of SABW still presented, illustrating that the crystalline structure was not completely destroyed and the material still has a certain mechanical strength. Importantly, MDI jade (XRD analysis software) was used to analyze the components of SABW (Fig. 2(b)), confirming the presence of $CaCO_3$ in SABW.

The infrared spectrum in (Fig. 2(c)) showed the successful modification of MPC. The spectrum of SABW exhibited new peaks at 710 cm^{-1} and 874 cm^{-1}, representing the deformation vibration peak of substituted benzene; and the peak at 1370 cm^{-1} belonging to the stretch vibration of tannin B ring.

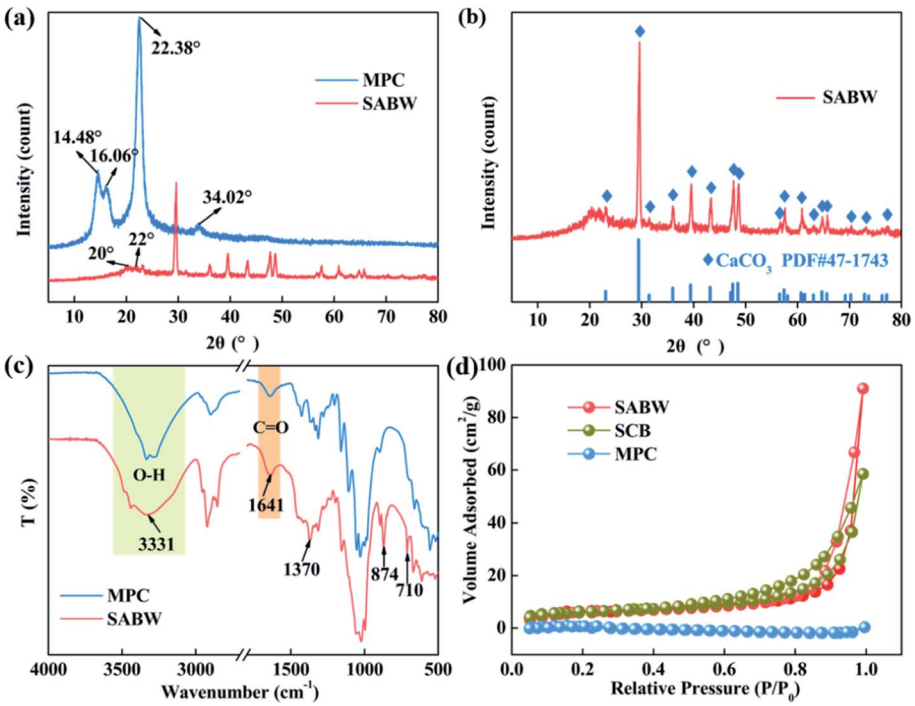

Fig. 2 XRD patterns of (a) MPC and SABW, (b) SABW analyzed by MDI jade. (c) The FT-IR spectra of MPC and SABW. (d) N_2 adsorption–desorption isotherms of MPC, SCB and SABW.

Table 1 Pore distribution properties of MPC, SCB and SABW

Sample	BET surface area ($m^2\ g^{-1}$)	Pore size (nm)	Pore volume ($cm^3\ g^{-1}$)
MPC	0.2718	—	—
SCB	19.92	17.91	0.0905
SABW	20.21	28.29	0.1409

According to the above analysis, black wattle extract has been successfully incorporated into the MPC skeleton (Table 6).

The BET surface areas of SCB and SABW was 19.92 $m^2\ g^{-1}$ and 20.21 $m^2\ g^{-1}$ respectively, which substantially higher than that of MPC (0.27 $m^2\ g^{-1}$) due to the method of dissolution and regeneration (Fig. 2(d) and Table 1). Meanwhile, the pore volume of SABW was higher than that of SCB, probably due to the presence of black wattle extract. The N_2 adsorption isotherms curves (Fig. 2(d)) revealed that SCB and SABW having the characteristics of a type H_3 hysteresis loop, indicating that the products were mesoporous materials.[34] With the modification on the MPC, SABW owned bigger pore size, which was consistent with the SEM analysis partially.

3.2 Adsorption experiments of GYP

3.2.1 Effect of pH values on the adsorption of GYP. The pH value of the liquid was an important controlling parameter in adsorption process.[35] As presented in Fig. 3(a), the adsorption efficiency and adsorption capacity of GYP increased with the increasing pH value in the range of 1.0–6.0, and gradually reduced in the range of 6.0 to 10.0. These facts implied that the sorption process was highly related to the pH value, and strong acidity or strong alkaline solution was not beneficial to the sorption. When the pH value was low (1.0), the surface of SABW was more protonated because of high concentration of hydrogen ions. GYP mainly existed in the form of cations in the solution, which would repel the positive charge on the adsorbent, resulting in relatively low adsorption capacity. As for the pH value of the solution was high, the adsorbent was more ionized by phenolic hydroxyl group, which greatly promotes the reaction of GYP and increased the adsorption capacity. Moreover, when the pH value was higher than pK_a value (4.21),[36] the GYP existed mostly as molecules in solution, which was contributed to the adsorption process. With the increase of solution pH, GYP was further deprotonized, resulting in a greatly reducing of electrostatic attraction.

In addition, the zeta potential tests indicated that the isoelectric point of SABW was 3.61 (Fig. 4). Therefore, when pH values lower than 3.61, the surface of SABW was protonated, and it became positively charged. This adsorbent surface exhibited an electrostatic repulsion with the cationic ions, leading to a decrease in the adsorption capacity of SABW. On the contrary, as the pH values increased above 3.61, the SABW was deprotonated, which contributed to an enhanced adsorption of GYP.

3.2.2 Kinetic studies. The effect of adsorption time on the adsorption was presented in Fig. 3(b). It was remarkable that SABW displayed an excellent adsorption performance. The equilibrium adsorption capacities increased rapidly within 80 min. In addition, the pseudo first- and second-order kinetic curves were shown in Fig. 5, and the correlation coefficient (R^2) as well as the calculated kinetic parameters were summarized in Table 2. And these data were fitted by pseudo-first-order kinetic model, pseudo-second-order kinetic model and intra-particle diffusion model. The R^2 of pseudo-first-order and pseudo-second-order kinetic equations were all relatively high (>0.99). However, the equilibrium adsorption capacity calculated by pseudo-first-order adsorption kinetic model was quite different from that measured by experiment, while the equilibrium

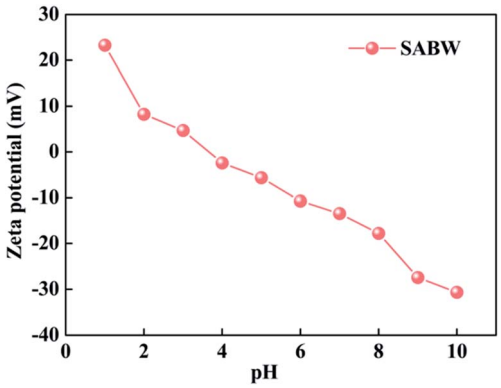

Fig. 4 Zeta potentials of SABW at various acidities (pH = 1–10).

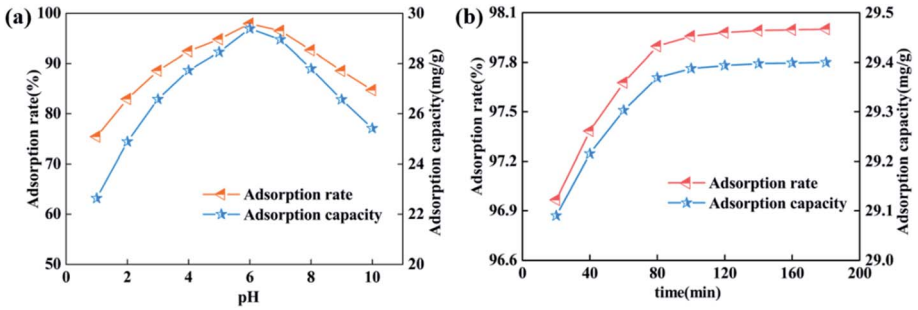

Fig. 3 (a) Effect of pH values on the adsorption, (b) effect of adsorption time on the adsorption. The initial concentration of GYP was 240 mg L^{-1}, the adsorption time was 180 min, the adsorbent usage was 0.2 g/25 mL, and the adsorption temperature was 30 °C.

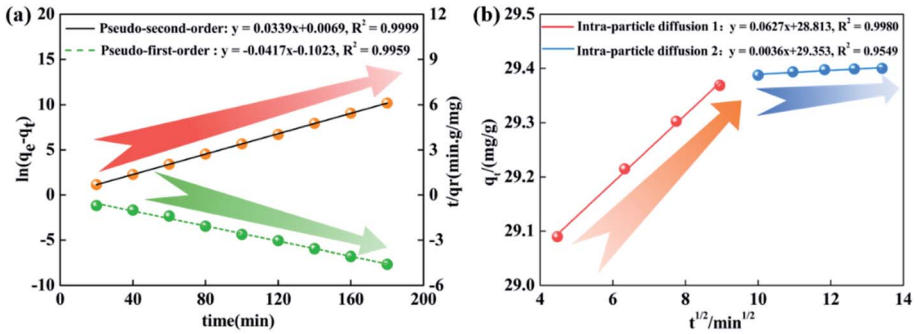

Fig. 5 (a) Pseudo-first-order and pseudo-second-order kinetic curves, (b) intra-particle diffusion kinetic curve.

Table 2 Kinetic equations and parameters

Dynamic equations	Dynamic parameters		R^2
Pseudo-first-order equation: $\ln(q_e - q_t) = \ln q_{e1} - k_1 t$	$k_1 = 0.0415$	$q_{e1} = 0.8899$ mg g^{-1} ($q_e = 29.39$ mg g^{-1})	0.9941
Pseudo-second-order equation: $t/q_t = 1/(k_2 Q_e^2) + t/Q_e$	$k_2 = 0.0340$	$Q_e = 29.41$ mg g^{-1} ($q_e = 29.39$ mg g^{-1})	0.9999
Intra-particle diffusion equation: $q_t = K_i t^{1/2} + C_i$	$K_1 = 0.0627$	$C_1 = 28.81$	0.9980
	$K_2 = 0.0036$	$C_2 = 29.35$	0.9549

adsorption capacity calculated by pseudo-second-order adsorption kinetic model was consistent with that measured by experiment. Therefore, the chemical adsorption took place during the adsorption process. The intra-particle curve was divided into two parts and was showed in Fig. 5(b). The first part was a straight line that did not pass through the origin, indicating that the intra-particle diffusion was not the only step to control the SABW adsorption process of GYP. The adsorption process was jointly controlled by surface diffusion and intra-particle diffusion.

3.2.3 Adsorption isotherms. In adsorption theories, Langmuir and Freundlich isotherms have been widely used to explain adsorption processes. According to the shape and change of adsorption isotherm, the relationship between adsorbents and adsorbates can be explored.[37,38] The relevant parameters could be seen in Table 3, the Langmuir and Freundlich isotherm model were all fit the experimental data, and the correlation coefficients (R^2) were higher than 0.995. Both saturated adsorption capacity (q_e) and Langmuir constant (b) increased with an increase of temperature, indicating that high temperature was conducive to the adsorption of GYP on SABW. The parameters K and $1/n$ obtained from the Freundlich model increased with the increased temperature, and the $1/n$ fell well in the range of 0.1–0.5, suggesting GYP adsorption of SABW was favorable and the adsorption effect was increased with increased temperature. The maximum adsorption capacity (Q_m) and the parameter of Langmuir (b) were related with initial adsorption concentrations and the properties of the adsorbent, respectively (Table 5). The b reflected the affinity or bonding strength between the adsorbent and the matrix.[39] The b value fitted by Langmuir model was relatively high, indicating that SABW had a good adsorption affinity for GYP. As previously mentioned, the surface morphology of SABW was relatively developed and the specific surface area was relatively high, which could provide more adsorption sites for targeted GYP molecule. Therefore, due to the introduction of tannin, the surface modification of MPC generally improved the adsorption

Table 3 Adsorption constants of GYP on SABW

Temperature (°C)	Langmuir isotherm model, $C_e/q_e = 1/(bQ_m) + C_e/Q_m$			Freundlich isotherm model, $\log q_e = \log K + 1/n \log C_e$		
	Q_m (mg g^{-1})	b (L mg^{-1})	R^2	K	$1/n$	R^2
30	37.17	0.4009	0.9984	14.95	0.2989	0.9981
40	39.06	0.4361	0.9988	15.31	0.3338	0.9970
50	40.16	0.4882	0.9970	16.04	0.3470	0.9986
60	40.65	0.5325	0.9989	16.60	0.3537	0.9990

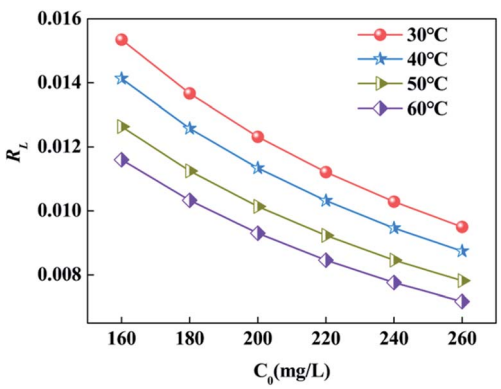

Fig. 6 The value of the equilibrium parameter R_L.

Table 4 The thermodynamics parameters for SABW adsorption on GYP

	Thermodynamics parameters		
Temperature (°C)	ΔG (kJ mol^{-1})	ΔH (kJ mol^{-1})	ΔS (kJ mol^{-1})
30	−37.75	8.08	124.6
40	−38.99		
50	−40.23		
60	−41.48		

percentage, affinity and sensitivity of GYP, which was conducive to the adsorption performance of adsorbent, and was suitable for the practical water remediation.

Furthermore, in order to confirm the adsorption of GYP by SABW, the dimensionless equilibrium parameter R_L (eqn (2)) was used to characterize the Langmuir adsorption isotherm:[40,41]

$$R_L = 1/(1 + bC_0) \quad (2)$$

where b is the parameter of Langmuir (mg L^{-1}), when $R_L > 1$, it is adverse adsorption; when $R_L = 1$, it is linear adsorption; when $R_L = 0$, it is irreversible adsorption; and when $0 < R_L < 1$, it is favorable adsorption, within this range, the R_L is larger, and the pollutants is better removal.

The equilibrium parameter (R_L) analysis in Fig. 6 showed that the R_L were less than 0.5 both in different concentrations and different temperatures, indicating that SABW had an efficient adsorption on GYP.

3.2.4 Adsorption thermodynamics. Adsorption temperature was a very important parameter in adsorption thermodynamics. Values of thermodynamic parameters such as Gibb's free energy (ΔG), enthalpy change (ΔH), and entropy change (ΔS) were further calculated by eqn (3) and (4) to measure the spontaneity of the adsorption process.[42–44]

$$\Delta G = \Delta H - T\Delta S \quad (3)$$

$$\ln(q_e/C_e) = \Delta S/R - \Delta H/RT \quad (4)$$

where R is the ideal gas constant 8.314 (J mol^{-1} K^{-1}) and T is the temperature (K).

The Langmuir and thermodynamics parameters for SABW adsorption on GYP were listed in Table 4. The ΔG values were negative and decreased with the increase of temperature, implying the spontaneity and feasibility of the sorption of GYP on the adsorbent. The value of ΔH was positive, indicated that the adsorption process was endothermic reaction. However, the positive ΔS values revealed that chaos increased during the reaction of GYP adsorption on SABW. This result confirmed that the temperature plays positive effects on GYP sorption process.

3.2.5 Desorption and reproducibility. Considering the cost of desorption and the safety of food pigment, in this part, 80% ethanol solution was selected as desorption solution to study the reuse ability of adsorbent SABW. The results of static adsorption/desorption experiments were shown in Fig. 7(e). After 4 times of reuse, the adsorption percentage could reach 92.30%, suggesting the excellent regeneration performance of SABW. In addition, the regenerated SABW had rough surface (Fig. 7(a–c)), which was conducive to the adsorption of GYP. Moreover, the morphological characteristics of SABW (Fig. 1(d–f)) and regenerated SABW were basically consistent, implying that the properties of regenerated cellulose did not change. Importantly, the spectrum of GYP-loaded SABW (denoted as SABW (GYP)) showed weaker peaks at 3331 cm^{-1} and 1641 cm^{-1} representing the deformation vibration peak of hydroxyl and carbon–oxygen double bond (Fig. 7(d)), implying the immobilization of GYP onto SABW. Moreover, the spectrum of SABW after desorption (denoted as SABW (re)) was the same as the spectrum of SABW (GYP), indicating that the adsorbent had very stable properties. These results implied that the adsorbent displayed outstanding regenerate .

3.3 Adsorption mechanism

The main adsorption mechanisms about GYP adsorption on SABW was explored (Fig. 8). The hydrogen bonding was hold to be an important mechanism in the adsorption process for GYP between the adsorbent and the adsorbate during the adsorption process. The FTIR results (Fig. 2(c)) clearly

Table 5 Comparison of the maximum adsorption capacity (q_e) of SABW on GYP with different forms of adsorbent

Adsorbent	q_e (mg g^{-1})	Reference
NKA macroporous resin	25.32	46
HPD_{450} resin	27.75	47
A-9 macroporous resin	1.22	48
A-5 macroporous resin	1.09	48
A-3 macroporous resin	1.02	48
A-1 macroporous resin	0.55	48
A-8 macroporous resin	0.32	48
A-2 macroporous resin	0.16	48
A-4 macroporous resin	0.16	48
A-7 macroporous resin	0.08	48
A-6 macroporous resin	0.06	48
A-10 macroporous resin	0.05	48
SABW	29.39	This work

Table 6 FT-IR characteristic peaks of main groups

Chemical bond	Wavenumber (cm^{-1})	Vibration mode
O–H	3700–3300	Stretching vibration
C=O	1900–1550	Stretching vibration
Substituted benzene	900–710	Deformation vibration
Tannins B ring	1600–1300	Stretching vibration

exhibited that SABW owned abundant H-bond donor and H-bond acceptor moieties, such as –OH, C=O groups, that means there could be a lot of hydrogen bonding between them. For example, the –OH of GYP react with the carbonyl groups for taking shape hydrogen bonds. Therefore, it could be illustrated that hydrogen bonding might play an important role in the adsorption of GYP on SABW. This meant that hydrogen bonding was one of the main mechanisms for the adsorption of GYP on SABW.

According to the characterization analysis of BET, the surface area of SABW was nearly a hundred times than MPC. Besides, previous results have reported that pore adsorption play an important role in adsorbing pollutants. Therefore, pore adsorption was thought to be exist between the SABW and GYP. As shown in Fig. 9(a and b), both MPC and SCB had a fairly low GYP adsorption capacity (<1.44 mg g^{-1}). Meanwhile, after normalized calculation of specific surface area, the adsorption capacity of SCB to GYP was lower than that of MPC, indicating that the BET surface area had little effect on the adsorption process and pore adsorption hardly work.

The adsorption of GYP on SABW was physicochemical process though electrostatic and ionic interactions between GYP and SABW. To explore the role of electrostatic interaction for the adsorption of GYP on SABW, the batch adsorption experiments were conducted at different pH values (1–10). As displayed in Fig. 3(a), the pH greatly influenced the adsorption performance of GYP on SABW. The equilibrium adsorption capacity of GYP should be the highest at pH = 6. When pH < 6, the equilibrium adsorption capacity was positively related to the acidity. Besides, when pH > 6, the equilibrium adsorption capacity was decreased with the increasing pH which due to the further deprotonized of GYP, resulting in a greatly reducing of electrostatic attraction. Moreover, from Fig. 9(c and d), SABW had a higher GYP adsorption capacity than SCB, and it was the same as after normalized calculation of specific surface area. These results indicated that tannins play a crucial role in GYP adsorption. Tannin was isoelectric at pH = 3.4,[45] the zeta potential changed from a positively charged to a negative charge, which was more attractive to negatively charged molecules. Therefore, it could be deduced that electrostatic interaction might play a very important role in the adsorption process.

As a consequence, the adsorption process of SABW on GYP involved three mechanisms like hydrogen bonding, pore adsorption, and electrostatic interaction.

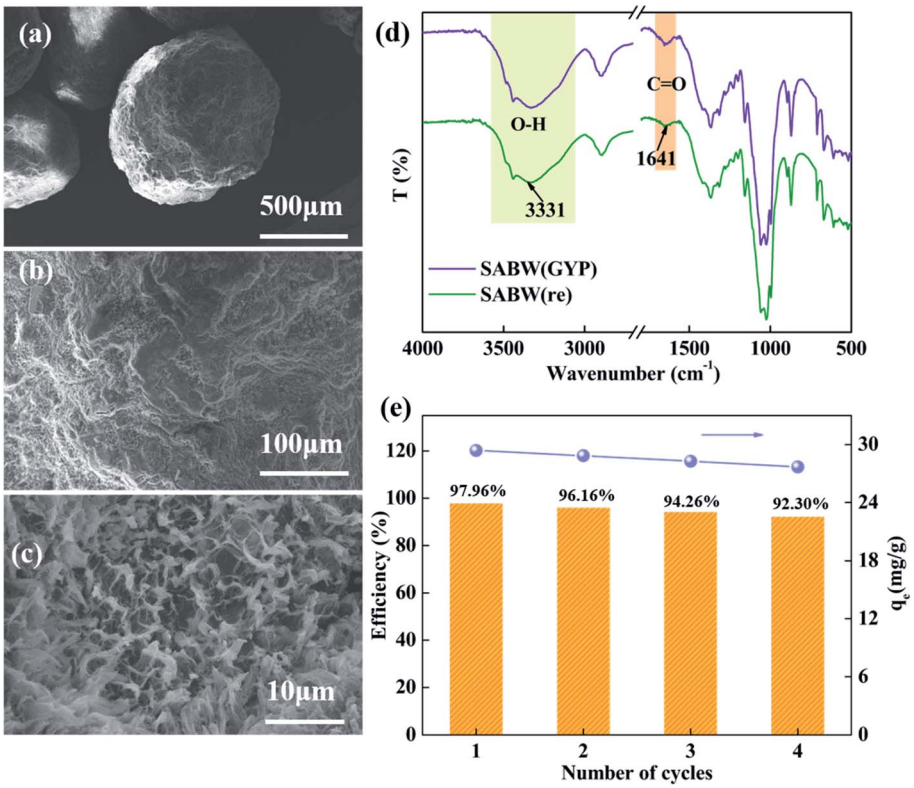

Fig. 7 (a–c) SEM images of regenerated SABW, (d) the FT-IR spectra of SABW (GYP) and SABW (re). (e) Reproducibility of SABW for GYP adsorption.

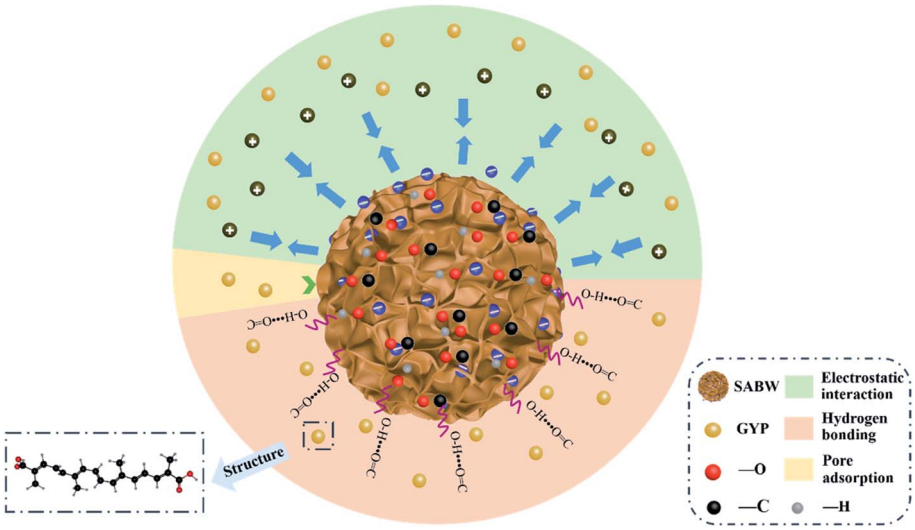

Fig. 8 Proposed synergetic mechanisms between SABW and GYP.

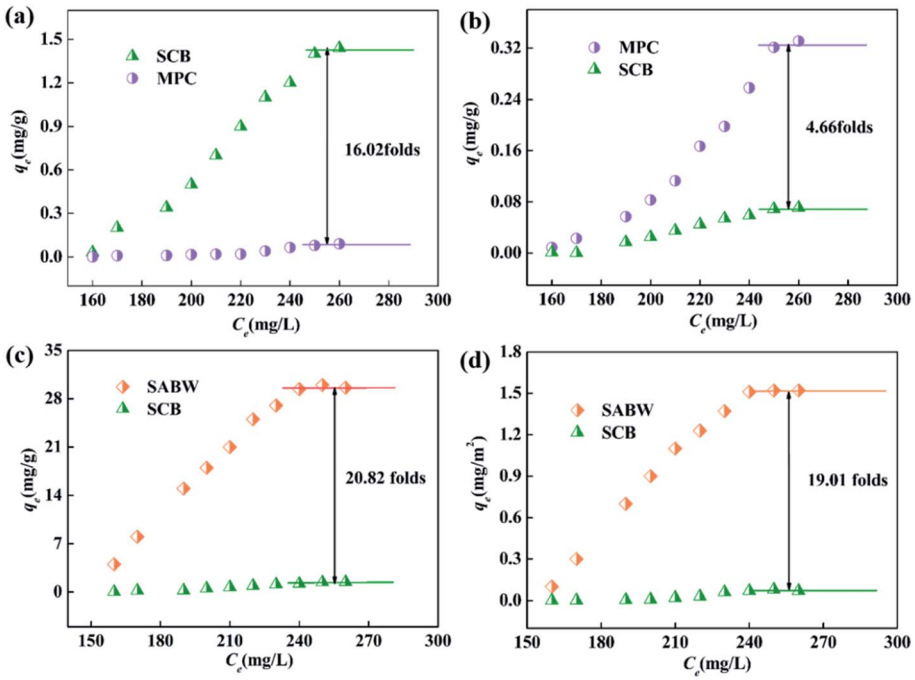

Fig. 9 Adsorption capacity of (a) MPC and SCB, (b) MPC and SCB in unit area, (c) SCB and SABW, (d) SCB and SABW in unit area.

4 Conclusions

An spherical cellulose adsorbent embedded with black wattle extract (SABW) was prepared by inverse suspension. Results of SEM, XRD, FTIR and BET characterization exhibited that SABW composed of abundant porous structure and functional groups such as –C═O, –OH and benzene ring groups. The adsorption results showed that the adsorption process followed the Langmuir and Freundlich isothermal adsorption model. Moreover, the static adsorption capacity of adsorbent to GYP could reach 97.96%, and the adsorption process was related to pH value, initial mass concentration and adsorption time. Studies on SABW desorption and regeneration showed that 80% ethanol as eluent could achieve good regeneration effect and retained 92.30% adsorption percentage after 4 cycles.

Conflicts of interest

There are no conflicts to declare.

Acknowledgements

The research was financially supported by National Science Foundation of China (No. 21577018) and the Open Foundation

of the Fujian Provincial Key Laboratory of Ecology-Toxicological Effects & Control for Emerging Contaminants (No. PY19003).

References

1 E. H. Park, M. H. Joo, S. H. Kim and C. J. Lim, Antiangiogenic activity of Gardenia jasminoides fruit, *Phytother. Res.*, 2010, **17**, 961–972.
2 S. P. Prabha, P. N. Ansil, A. Nitha, P. J. Wills and M. S. Latha, Preventive and curative effect of methanolic extract of Gardenia gummifera Linn. f. on thioacetamide induced oxidative stress in rats, *Asian Pac. J. Trop. Dis.*, 2012, **2**, 90–98.
3 X. H. Wei, X. M. Cheng, J. S. Shen and Z. T. Wang, Antidepressant effect of Yueju-Wan ethanol extract and its fractions in mice models of despair, *J. Ethnopharmacol.*, 2008, **117**, 339–344.
4 Q. C. Chen, W. Y. Zhang, H. J. Kim, I. S. Lee, Y. Ding, U. J. Youn, S. M. Lee, M. K. Na, B. S. Min and K. H. Bae, Effects of gardeniae fructus extract and geniposide on promoting ligament cell proliferation and collagen synthesis, *Phytother. Res.*, 2010, **24**, S1–S5.
5 H. J. Koo, S. Lee, K. H. Shin, B. C. Kim and E. H. Park, Geniposide, an anti-angiogenic compound from the fruits of Gardenia jasminoides, *Planta Med.*, 2004, **70**, 467–469.
6 S. J. Lee, P. S. Oh, J. H. Ko and K. Lim, Glycoprotein isolated from Gardenia jasminoides Ellis has a scavenging activity against oxygen radicals and inhibits the oxygen radical-induced protein kinase C alpha and nuclear factor-kappa B in NIH/$_3$T$_3$ cells, *Environ. Toxicol. Pharmacol.*, 2006, **21**, 8–21.
7 K. H. Park, T. Y. Kim, J. Y. Park, E. M. Jin and J. W. Lee, Photochemical properties of dye-sensitized solar cell using mixed natural dyes extracted from Gardenia Jasminoide Ellis, *J. Electroanal. Chem.*, 2013, **689**, 21–25.
8 J. G. Yang, Y. H. Shen, Y. Hong, F. H. Jin, S. H. Zhao, M. C. Wang, X. J. Shi and X. Fang, Stir-baked Fructus gardeniae (L.) extracts inhibit matrix metalloproteinases and alter cell morphology, *J. Ethnopharmacol.*, 2008, **117**, 285–289.
9 B. Yang, X. Liu and Y. Gao, Extraction optimization of bioactive compounds (crocin, geniposide and total phenolic compounds) from Gardenia (Gardenia jasminoides Ellis) fruits with response surface methodology, *Innovative Food Sci. Emerging Technol.*, 2009, **10**, 610–615.
10 H. P. Zhang, J. Y. Guo and T. Li, Selective separation of geniposide and gardenia yellow from gardenia fruit by isopropanol/salt aqueous two-phase system, *Sep. Sci. Technol.*, 2016, **51**, 1–9.
11 T. Watanabe and S. J. Terabe, Analysis of natural food pigments by capillary electrophoresis, *Chin. J. Chromatogr.*, 2000, **880**, 311–322.
12 L. L. Li, S. Zhao and H. Wang, Optimization of Ultrasonic Assisted Extraction of Geniposide from Gardenia Fruits by Using Ethanol/Salt Aqueous Two-phase System with Response Surface Method, *Chem. Ind. For. Prod.*, 2017, **2**, 97–104.
13 L. Xiong and Q. W. Chen, The Supercritical CO_2 Fluid Extraction of Gardenia Yellow Pigment, *J. Hunan Agric. Univ.*, 2010, **49**, 85–87.
14 Z. J. Ren, K. Z. He and J. Tan, Purification of Gardenia Yellow by Macroporous Adsorption Resin, *J. Food Sci.*, 2005, **26**, 157–162.
15 R. Chen, J. Shui and R. Liang, Study on Extraction Technology of Gardenia Yellow Pigment by Dynamic Extraction, *For. Prod. Spec. Chin.*, 2016, **4**, 9–14.
16 L. Peng, K. J. Fan and Q. P. Xiong, Optimization of Separation and Purification Technology for Gardenoside from Extraction Liquid of Gardenia jasminoides by Macroporous Resin, *Chin. J. Exp. Tradit. Med. Formulae*, 2012, **22**, 30–34.
17 L. P. Zhang, J. Liu and G. W. Chen, Preparation of Macroporous Adsorption Resin of Immobilized Tannins and Its Adsorption Behavior, *Chem. Ind. For. Prod.*, 2007, **5**, 70–75.
18 I. A. Sengil, M. Oezacar and H. J. Tuerkmenler, Kinetic and isotherm studies of Cu(II) biosorption onto valonia tannin resin, *J. Hazard. Mater.*, 2009, **162**, 1046–1052.
19 Y. Nakano, K. Takeshita and T. Tsutsumi, Adsorption mechanism of hexavalent chromium by redox within condensed-tannin gel, *Water Res.*, 2001, **35**, 500.
20 C. G. He, P. Liu and Y. Liao, Adsorption Property of Tannins Immobilized by Collagen Fiber on La^{3+}, *J. Chin. Rare Earth Soc.*, 2007, **25**, 274–278.
21 S. D. Chen, W. J. Fang and L. M. Xie, Study on adsorption properties of immobilized tannins for nutrients in wine, *J. Zhejiang Univ., Sci., B*, 2003, **30**, 666–670.
22 L. Li, F. Q. Zhou and T. Tian, Preparation of a New Tannins Immobilized Macroporous Resin and Its Adsorption Behavior Towards Pd(II), *J. Anal. Sci.*, 2009, **25**, 193–196.
23 Y. Pei, G. Q. Xu and X. Wu, Removing Pb(II) Ions from Aqueous Solution by a Promising Absorbent of Tannin-Immobilized Cellulose Microspheres, *Polymers*, 2019, **11**, 548–559.
24 G. Zheng, W. J. Deng and J. W. Luo, Multifunctional nanocellulose composite films with grape seed extracts and immobilized silver nanoparticles, *Carbohydr. Polym.*, 2018, **205**, 447–455.
25 Y. Anna, J. Adam and C. J. Daria, Significant enhancement of citric acid production by Yarrowia lipolytica immobilized in bacterial cellulose-based carrier, *J. Biotechnol.*, 2020, **321**, 13–22.
26 I. Jilal, S. E. Barkany, Z. Bahari, O. Sundman and H. Amhamdi, New quaternized cellulose based on hydroxyethyl cellulose (HEC) grafted EDTA: synthesis, characterization and application for Pb (II) and Cu (II) removal, *Carbohydr. Polym.*, 2018, **180**, 156–167.
27 S. Y. Tian, J. H. Guo, C. Zhao, Z. Peng and C. H. Gao, Preparation of Cellulose/Graphene Oxide Composite Membranes and Their Application in Removing Organic Contaminants in Wastewater, *J. Nanosci. Nanotechnol.*, 2019, **4**, 2147–2153.
28 X. F. Zhang, X. D. Cao, B. Zhu, X. Zhang and D. Hua, Polymyxin B immobilized on cross-linked cellulose

microspheres for endotoxin adsorption, *Carbohydr. Polym.*, 2016, **136**, 12–18.

29 X. J. Peng and Z. G. Li, Determination of geniposide in the processed products of Fructus Gardeniae by HPLC, *West China J. Pharm. Sci.*, 2005, **20**, 549.

30 C. Lin, H. Zhan, M. Liu, J. Zhang and S. Fu, Thermodynamics and kinetics of adsorption of Cu (II) from aqueous solutions onto a spherical cellulose adsorbent, *Ion Exch. Adsorpt.*, 2010, **26**, 226–238.

31 Y. Chen, X. Jiang and H. Wu, Thermal behavior of complex model with the cellulose II and amorphous chain, *J. Theor. Comput. Chem.*, 2020, **19**, 25–42.

32 G. K. Li, Studies on the Preparation and Characterization of Nano-Crystal Cellulose II, *J. Cellul. Sci. Technol.*, 2002, **2**, 14–21.

33 F. Khili, J. Borges and P. L. Almeida, Extraction of Cellulose Nanocrystals with Structure I and II and Their Applications for Reduction of Graphene Oxide and Nanocomposite Elaboration, *Waste Biomass Valorization*, 2019, **10**, 1913–1927.

34 Y. Liu and S. R. Mo, Progress in Study of Gardenia Yellow Pigment, *Chin. J. Ethnomed. Ethnopharm.*, 2007, **88**, 265–268.

35 X. Y. Li, V. T. John and J. H. He, The synthesis of mesoporous $TiO_2/SiO_2/Fe_2O_3$ hybrid particles containing micelle-induced macropores through an aerosol based process, *Langmuir*, 2011, **27**, 6252–6259.

36 T. C. Christian, F. Henri and P. Catherine, Removal of Cd(II) and Pb(II) ions, from aqueous solutions, by adsorption onto sawdust of Pinus sylvestris, *J. Hazard. Mater.*, 2003, **105**, 121–142.

37 Q. Song, Z. Wu and W. J. Xie, Adsorptive recovery of geniposidic acid from gardenia yellow pigment extraction wastewater by anion exchange: equilibrium, thermodynamics and mechanism modeling and simulation, *Res. Chem. Intermed.*, 2017, **43**, 2215–2235.

38 A. Guenay, E. Arslankaya and I. Tosun, Lead removal from aqueous solution by natural and pretreated clinoptilolite: adsorption equilibrium and kinetics, *J. Hazard. Mater.*, 2007, **146**, 362–371.

39 A. Saqr, E. Q. Amjad, A. Q. Hana, H. Maryam and A. Z. Wessal, Effective adsorptive removal of Zn^{2+}, Cu^{2+}, and Cr^{3+} heavy metals from aqueous solutions using silica-based embedded with NiO and MgO nanoparticles, *J. Environ. Manage.*, 2020, **268**, 110713–110724.

40 N. Daneshvar, D. Salari and S. Aber, Chromium adsorption and Cr(VI) reduction to trivalent chromium in aqueous solutions by soya cake, *J. Hazard. Mater.*, 2002, **94**, 49–61.

41 T. S. Singh, K. Pant and P. Technology, Equilibrium, kinetics and thermodynamic studies for adsorption of As(III) on activated alumina, *Sep. Purif. Technol.*, 2004, **36**, 139–147.

42 A. Sari, M. Tuzen, D. Ctak and M. J. Soylak, Adsorption characteristics of Cu(II) and Pb(II) onto expanded perlite from aqueous solution, *J. Hazard. Mater.*, 2007, **148**, 387–394.

43 A. Sari and M. Tuzen, Removal of Cr(VI) From Aqueous Solution by Turkish Vermiculite: Equilibrium, Thermodynamic and Kinetic Studies, *Sep. Sci. Technol.*, 2008, **43**, 3563–3581.

44 E. Mildan and M. Gülfen, Equilibrium, kinetics, and thermodynamics of Pd(II) adsorption onto poly(m-aminobenzoic acid) chelating polymer, *J. Appl. Polym. Sci.*, 2015, **132**, 42533–42542.

45 S. Szymon, O. G. Ewa and W. Wieckowska, Spectroscopic, Zeta-potential and Surface Plasmon Resonance analysis of interaction between potential anti-HIV tannins with different flexibility and human serum albumin, *Colloids Surf., B*, 2020, **194**, 111175–111184.

46 C. P. Wang, J. B. Ji and L. H. Wang, Separation of Gardenia yellow with NKA macroporous adsorption resin, *Chem. Prog.*, 2003, **6**, 72–75.

47 Z. S. Zhong, J. X. Pan and Y. K. Chen, High color value of gardenia yellow refined, *Fine Chem. Ind.*, 2007, **6**, 581–591.

48 D. Q. Zhang, F. J. Lv, J. X. Tai and Q. Fu, Purification of gardenia yellow pigment with macroporous resin, *J. Agric. Eng.*, 2004, **4**, 165–167.